JOURNAL OF GEOPHYSICAL RESEARCH, VOL. 102, NO. B9, PAGES 20,199–20,210, SEPTEMBER 10, 1997

Thermoremanence, anhysteretic remanence and susceptibility of submicron magnetites: Nonlinear field dependence and variation with grain size

David J. Dunlop and Kenneth S. Argyle[1]

Geophysics Laboratory, Department of Physics, University of Toronto, Mississauga, Ontario, Canada

Abstract. We have measured initial susceptibility χ_o and the dependence of anhysteretic remanent magnetization (ARM) and thermoremanent magnetization (TRM) on applied field for seven samples of magnetite, with mean grain sizes from 40 to 540 nm. TRM acquisition is nonlinear in geomagnetically relevant weak fields, contrary to the usual assumption made in paleointensity determination. Over the 40-540 nm range, χ_o varies with particle shape but only weakly with particle size d and can be used to correct for varying magnetite concentrations in sediment cores. ARM is strongly size dependent over the same range and is the best parameter for monitoring grain size variations in natural samples. ARM and TRM have similar variations, as d^{-1} for $d \leq 1$ μm, suggesting a common source for this pseudo-single-domain (PSD) dependence on grain size. However, TRM is 10-20 times more intense than ARM in grains around 0.2 μm in size. The TRM microstate seems to be a two-domain structure, whereas the ARM microstate may be a vortex structure, which has never before been convincingly demonstrated by magnetic measurements. Independent evidence comes from theoretical fits to TRM and ARM field dependence data. In moderate and strong fields, TRM in 215-540 nm magnetites is explained by two-domain theory, but ARM is not. In smaller grains ($d \leq 0.1$ μm), a PSD theory predicts that TRM is carried by single-domain (SD) moments of entire grains but ARM resides in moments (≈ 1 per grain) 20-40 times weaker. These remanence levels match those of (metastable) SD and vortex states, respectively. We therefore propose that magnetite grains in the 0.1-0.5 μm size range can remain in metastable SD or two-domain states following acquisition of TRM but revert to a vortex ground state when field-cycled, for example, in ARM acquisition or alternating field demagnetization.

Introduction

Thermoremanent magnetization (TRM) is the primary remanence of igneous rocks. It is produced over an interval of blocking temperatures during cooling from the Curie point in a magnetic field and can be progressively unblocked or thermally demagnetized by reheating in zero field. Anhysteretic remanent magnetization (ARM) is produced when a steady or slowly varying field is superimposed on a decaying alternating field (AF) of higher frequency and mimics the bias analog recording process. The reciprocal erasure process is AF demagnetization.

ARM does not occur in nature, but laboratory-produced ARM is of interest in rock magnetism as an analog to TRM. In analog ARM/TRM theories [*Jaep*, 1969, 1971; *Banerjee and Mellema*, 1974; *Stephenson and Collinson*, 1974], the alternating field has a randomizing effect in ARM and AF demagnetization similar to that of thermal fluctuations in TRM and thermal demagnetization. Experimentally, AF demagnetization curves of ARM and TRM in magnetite are quite similar [*Dunlop and West*, 1969; *Dunlop et al.*, 1973; *Levi and Merrill*, 1976], although with significant differences at low coercivities [*Dunlop and Argyle*, 1991]. The ratio of intensities of TRM and ARM produced by the same steady field, on the other hand, is quite variable and reaches large values (≥ 10) around 200 nm [*Dunlop et al.*, 1975; *Levi and Merrill*, 1976; *Bailey and Dunlop*, 1977], just above the critical single-domain (SD) size d_0 (50-80 nm) [*Dunlop*, 1973a; *Enkin and Williams*, 1994].

The preferred micromagnetic structure of magnetite crystals around 200 nm in size is not entirely clear. The volume that is thermally activated in 220 nm crystals during TRM acquisition, TRM demagnetization, and high-temperature hysteresis corresponds to the expected volume of the domain wall in a two-domain (2D) structure (see *Dunlop* [1977] for a summary). The 2D structure is one of the permitted local energy minimum (LEM) states [*Moon and Merrill*, 1984] for 200 nm model magnetite cubes, along with quasi-SD or "flower," curling or vortex, and at least two other states [*Williams and Dunlop*, 1989, 1990, 1995]. The vortex state has the lowest energy for all sizes above d_0 [*Thomson et al.*, 1994], and other initial structures revert to this state during simulated room-temperature hysteresis [*Williams and Dunlop*, 1995].

ARM acquisition involves repeated cycling through the hysteresis loop, so 200 nm grains should theoretically be in low-remanence vortex states after this process. In TRM acquisition, the experimental evidence favors a 2D state with a substantial domain-wall moment in 220 nm grains [*Dunlop*, 1977]. The very different net moments of the high-temperature and low-temperature states would account for the contrast between TRM and ARM intensities. In general support of this idea, Monte Carlo calculations simulating the effect of thermal fluctuations suggest that magnetite grains below ≈500 nm

[1]Now at Arlat Inc., Bramalea, Ontario, Canada.

Paper number 97JB00957.
0148-0227/97/97JB-00957$09.00

in size will revert to a vortex state, while larger grains can preserve conventional domain structures [*Fukuma and Dunlop*, 1997].

There is almost no published information on ARM and TRM intensities in magnetites 200-500 nm in size. The data in this paper are intended to fill that gap. They show that the pseudo-single-domain (PSD) grain-size dependences of TRM and ARM established for smaller grains continue smoothly in the 200-500 nm range and link with data for 1 μm and larger grains. The new data also make it possible to test existing theories of TRM and ARM acquisition.

Samples and Experiments

The three main samples, A1, A2, and A3, used in our work are ≈1.3% by volume dispersions in a clay matrix of magnetites produced by reducing commercial Mapico "cubic" hematites originally prepared by oxidizing a cubic spinel phase. Curie temperature T_C, saturation magnetization M_s, and X ray diffraction lines of the reduced material agreed closely with standard values for pure magnetite [see *Argyle and Dunlop,* 1990, Tables 1 and 2]. Scanning electron micrographs showed that the grains were subhedral and approximately equidimensional, with mean sizes and ±1σ dispersions of 215 ± 78 nm (A1), 390 ± 112 nm (A2), and 540 ± 185 nm (A3). Room-temperature values of coercive force H_c and saturation remanence ratio M_{rs}/M_s followed standard hydrothermal trends [*Dunlop,* 1986; *Heider et al.*, 1987; see *Argyle and Dunlop,* 1990, Figures 3 and 4]. All samples were thoroughly outgassed at 350°C and vacuum annealed for several hours at 650°-700°C prior to beginning experiments to stabilize their properties.

The properties of five other samples are described in this paper for comparison with those of A1-A3. D1-D4 are ≈1% by volume dispersions of the same magnetites used by *Dunlop* [1973a,b, 1986], which are single-crystal cubes grown in aqueous solution with mean sizes of 220, 100, 76, and 37 nm, respectively, and size dispersions of 30-40% about the mean [see *Dunlop*, 1986, Table 1 and Figure 1]. TRMs of samples D1-D4 have been described previously [*Dunlop*, 1973b] but ARM's have not. Sample M1 containing "Mapico Black" magnetite, with mean size 215 nm, was also measured for comparison with other studies [*Levi and Merrill*, 1976, 1978]. Vacuum annealing had a small effect on the hysteresis properties of D1-D4 but a large effect on the properties of M1, which after annealing became almost identical to those of D1 and A1.

ARMs were produced by the combined steady field $\mathbf{H}_o$ of a small solenoid and the smoothly decaying AF of a large demagnetizing coil with initial peak field 100 mT. A variety of different steady fields were used, ranging from 50 μT to 1.7 mT for A1-A3 and M1 and from 100 μT to 4 mT for D1-D4. TRMs were produced in vacuum heatings in a noninductive furnace using steady fields H_o of 50 μT to 1.7 mT for A1-A3 and M1 and 100 μT to 9 mT for D1-D4. TRM intensities, hysteresis parameters, and AF demagnetization curves were reproducible to within a few percent after the complete set of heatings.

Measurements of ARM, M_{ar}, and TRM, M_{tr}, were made with spinner (A1-A3, M1) or ballistic (D1-D4) magnetometers. Hysteresis, including the initial magnetization (M-H_o) curve from an AF demagnetized state, was either measured with the same magnetometer (D1-D4) or with a vibrating-sample magnetometer cross-calibrated to the spinner through measurements of saturation remanence, M_{rs} (A1-A3, M1). In this way, TRM susceptibility χ_{tr}, ARM susceptibility χ_{ar}, and DC initial susceptibility χ_o could be confidently compared; such comparisons are difficult if χ_o is measured with a susceptibility bridge. AF demagnetization of A1-A3 was carried out along three orthogonal axes in succession with the same demagnetizer used to produce ARMs.

ARM, TRM, and Initial Susceptibility Data

ARM, TRM, and DC initial magnetization properties of the experimental samples are compared in Table 1. The listed susceptibilities $\chi_o = dM/dH_o$, $\chi_{ar} = dM_{ar}/dH_o$, and $\chi_{tr} = dM_{tr}/dH_o$ are values determined for a field H_o of 1 Oe or $1000/4\pi = 79.6$ A/m ($\mu_o H_o = 0.1$ mT). Note that because the conversion of magnetizations, M= 1 emu/cm^3= 1000 A/m, does not match the conversion of H_o, SI values of all susceptibilities are a factor 4π larger than cgs values. Note also that the intensities of ARM and TRM plotted in Figures 1 and 2, with values of M_{tr} or M_{ar} in kA/m (i.e., emu/cm^3) for an inducing field $\mu_o H_o$ of 0.1 mT (i.e., H_o= 1 Oe), correspond to cgs values of χ_{tr} or χ_{ar}.

Size dependence of initial susceptibility. Initial susceptibility χ_o is only slightly size dependent over the range 37-540 nm. Our measured χ_o values vary from about 0.24-0.47 (cgs) or 3-6 (SI), similar to the range 0.20-0.32 (cgs) or 2.5-4 (SI) determined by *Heider et al.* [1996] over a very broad size span in equidimensional hydrothermal magnetites. Heider et al. modeled cylindrical particles over the size range 50-120 nm in which quasi-SD and vortex structures are competing LEM states and predicted χ_o values between about 2 and 3 (SI) for equidimensional particles and between about 2 and 4 for particles with 2:1 elongation. The values we measure for equant 37-100 nm grains are 3-3.5, slightly higher than their predictions.

If our larger grains (samples D1, M1, A1-A3) are in 2D states, their susceptibilities due to wall motion limited by self-demagnetization would be ≤1/N = 0.62 (cgs) or 7.8 (SI) (see *Dunlop* [1983] or *Xu and Merrill* [1987] for calculations of the demagnetizing factor N of a 2D cube). Elongated particles would have even higher susceptibilities. Since our values are all well below this limit, wall motion must be strongly impeded in these submicron particles, as one would anticipate from their large values of H_c compared to those of ≥1 μm particles. Alternatively, some or all of the grains may be in states other than 2D.

Whatever the LEM state, χ_o increases with particle elongation. Experimentally, we see this effect clearly in comparing samples D1, M1 and A1, all of which have a nominal mean grain size of 215-220 nm. The grains in D1 are almost perfect cubes, those in M1 are less perfect cubes, while those in A1 are somewhat elongated [cf. *Dunlop*, 1986, Figure 1; *Argyle and Dunlop,* 1990, Figure 1]. The corresponding χ_o values are 3.67, 4.12, and 5.94 (SI), respectively.

Size dependence of ARM. With a large AF helping grains overcome barriers to reversals of moments or displacements of walls, the in-field anhysteretic susceptibility $\chi_a = dM_a/dH_o$ should be larger than χ_o due to H_o alone. However, when H_o is switched off, domain walls tend to spring back to positions close to the demagnetized

Table 1. Initial Susceptibilities and ARM and TRM Properties of the Experimental Samples

Sample	<d>, nm	χ_o, cgs	χ_o, SI	χ_{ar}, cgs	χ_{ar}, SI	$Q_a = \chi_{ar}/\chi_o$	χ_{tr}, cgs	χ_{tr}, SI	$Q_t = \chi_{tr}/\chi_o = Q_t/Q_a$	χ_{tr}/χ_{ar}
A3	540	0.370	4.65	0.156	1.96	0.42	1.25	15.7	3.4	8.0
A2	390	0.400	5.03	0.312	3.92	0.78	3.22	40.5	8.0	10.3
A1	215	0.473	5.94	0.416	5.23	0.88	7.33	91.7	15.5	17.6
M1	215	0.328	4.12	0.420	5.28	1.28	5.3	66.6	16.2	12.6
D1	220	0.292	3.67	0.416	5.23	1.42	8.0	101	27.4	19.2
D2	100	0.280	3.52	1.07	13.4	3.82	12.5	157	44.6	11.7
D3	76	0.268	3.37	1.30	16.3	4.85	11.8	148	44.0	9.1
D4	37	0.236	3.00	1.74	21.9	7.37	6.0	75.4	25.4	3.45

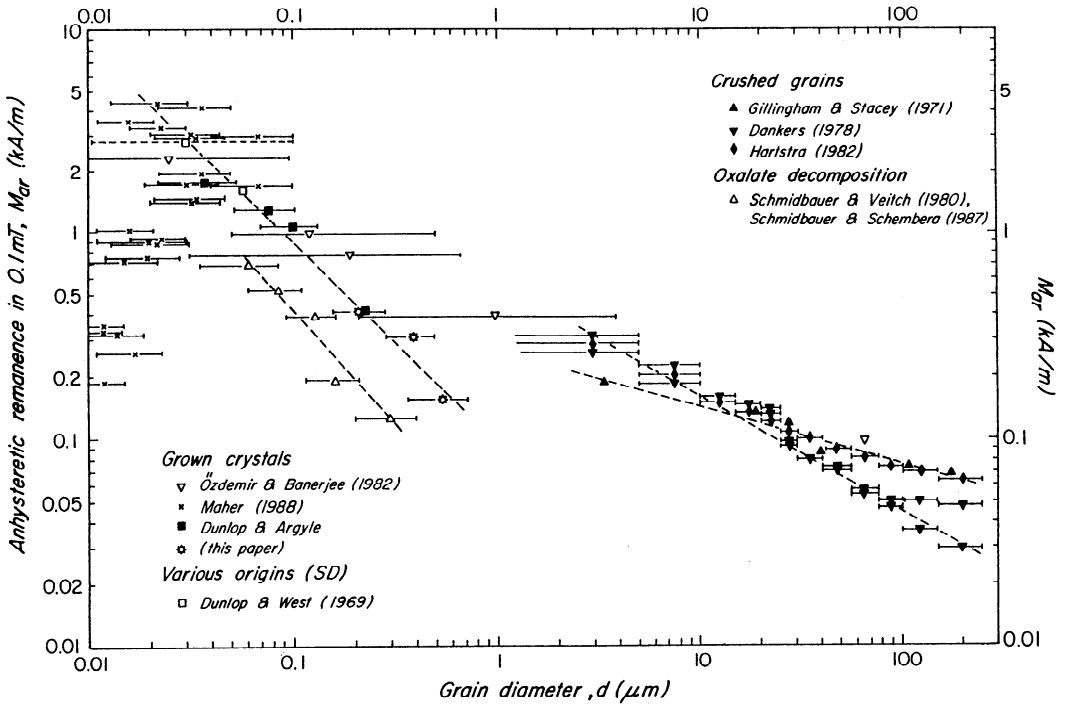

Figure 1. Weak-field ARM as a function of magnetite grain size d. M_{ar} varies as d^{-1} between the SD threshold d_o and ≈1 μm, based mainly on the data in this paper and the data of *Dunlop and West* [1969], and less strongly (as $d^{-0.27}$ to $d^{-0.55}$) above 1 μm.

state. As a result of this self-demagnetization, χ_{ar} is comparable to χ_o in larger grains (Table 1). In ≤100 nm grains, on the other hand, χ_{ar} is 4 to 7 times larger than χ_o. In these smaller grains, ARM seems to reside in vortex or SD-like moments which are strongly pinned compared to walls and do not self-demagnetize when $H_o \to 0$. If this interpretation is correct, we may be able to use ARM measurements to pinpoint the first appearance of walls or wall-like structures such as pairs of linked vortices [*Newell et al.*, 1993; *Fabian et al.*, 1996] in magnetite as the grain size increases above d_o. Table 1 suggests that a threshold value of the "anhysteretic Koenigsberger ratio," $Q_a = \chi_{ar}/\chi_o$, is 1-2 and the threshold size for walls is ≈200 nm.

When compared to a compilation of published ARM measurements (Figure 1), our data for A1-A3, M1, and D1-D4 confirm the

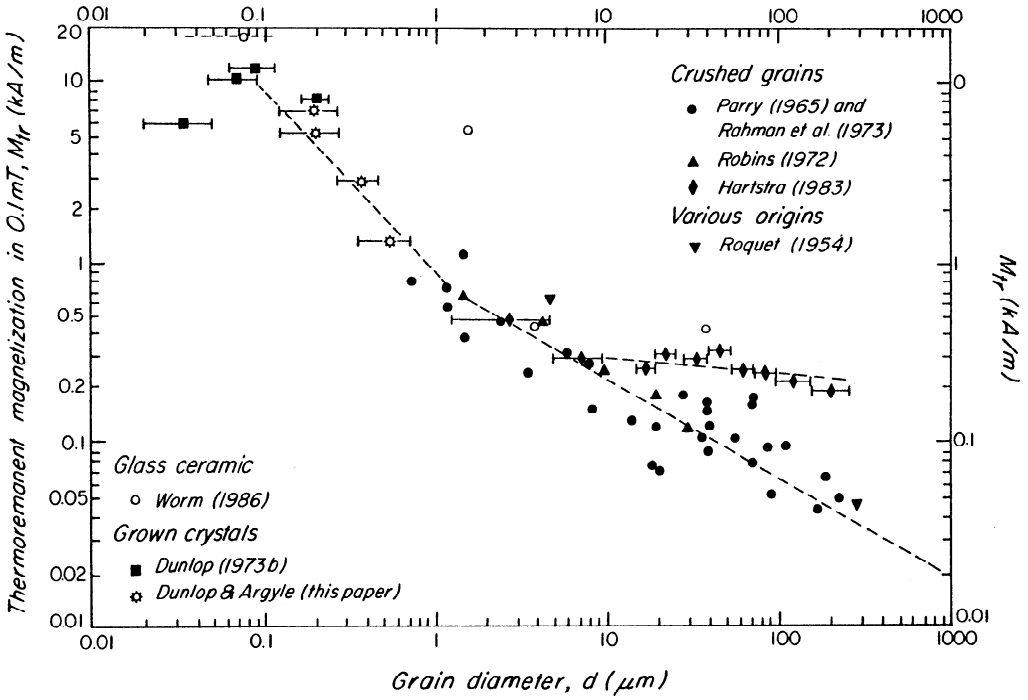

Figure 2. Weak-field TRM as a function of magnetite grain size d. M_{tr} varies as d^{-1} between d_o and ≈1 μm, based mainly on the data in this paper and of *Dunlop* [1973b], and less strongly (as $d^{-0.55}$ or weaker) above 1 μm. The two trends merge smoothly, unlike the corresponding ARM trends in Figure 1.

PSD trend of decreasing χ_{ar} values in magnetite as the grain size increases from SD to ≥1 μm [e.g., *Dunlop and West*, 1969; *Özdemir and Banerjee*, 1982]. ARM is known to be strongly concentration dependent [*Sugiura*, 1979], so it is important to compare samples with similar volume fractions of magnetite. For our samples and those of *Dunlop and West* [1969], the magnetite concentration was ≈1% by volume. *Schmidbauer and Schembera* [1987] used a higher concentration (3% by volume) and a nonhydrothermal preparation method. Their M_{ar} values are lower than ours and lie on a parallel trend. The data of *Maher* [1988] are rather scattered. In part, this may reflect the varying magnetite concentrations in different samples, but the very low values at the smallest particle sizes are due to superparamagnetic particles.

On the basis of our data and those of *Dunlop and West* [1969], M_{ar} varies with grain size d approximately as d^{-1} over the size range 30-540 nm. *Özdemir and Banerjee*'s [1982] three smallest magnetites and most of *Maher*'s [1988] larger magnetites have M_{ar} values on or near the same trend line. M_{ar} is less strongly dependent on grain size in 3-200 μm magnetites, varying as $d^{-0.55}$ according to the data of *Dankers* [1978] and *Potter and Stephenson* [1986] (not shown), or as $d^{-0.27}$ according to the data of *Gillingham and Stacey* [1971], *Hartstra* [1982], and *Dunlop and Xu* [1993] (not shown). The magnetites used by all these authors were crushed from larger crystals and have considerable internal stress, particularly the smaller grains. Dislocations and other defects pin domain walls, decreasing χ_o but increasing M_{ar} compared to hydrothermal or other low-stress magnetites of the same size. It is probably for this reason that the ≤1 μm (hydrothermal) and ≥1 μm trends do not merge in Figure 1. Trends in χ_o, H_c, H_{cr} (remanent coercive force), and M_{rs} data for hydrothermal and crushed magnetites have similar incompatibilities [*Dunlop*, 1986; *Heider et al.*, 1987, 1996; *Argyle and Dunlop*, 1990; *Hunt et al.*, 1995].

Size dependence of TRM. In TRM acquisition, random thermal fluctuations at the blocking temperature T_B overcome barriers to wall motions or reversals of SD or vortex moments, the steady field $\mathbf{H_o}$ acting mainly as a bias. Although the AF in principle plays the same role in ARM as thermal excitations do in TRM, the TRM acquisition process is much more efficient, at least in fine grains like ours. Values of χ_{tr} range from 1-12 (cgs) or 15-150 (SI) and are much larger than either χ_o or χ_{ar} for the same sample (Table 1). The Koenigsberger ratio $Q_t = \chi_{tr}/\chi_o$ ranges from 3 to 45, much above the value 0.5-1 expected for multidomain grains with wall motion limited solely by self-demagnetization. High values of Q_t were one of the criteria used by *Stacey* [1967] in defining PSD behavior.

There are few published TRM data sets (see *Day* [1977] for a review) and no previous data for magnetites between 200 and 700 nm in size. Our data for samples A1-A3 and M1 span the gap between M_{tr} values for sample D1 (220 nm [*Dunlop*, 1973b]) and 800 nm crushed magnetites [*Rahman et al.*, 1973], which differ by about an order of magnitude (Figure 2). Overall M_{tr} varies very nearly as d^{-1} over the range 80 nm to 1 μm, based on data for D1-D3, M1, A1-A3, and the smaller magnetites of *Robins* [1972] and *Rahman et al.* [1973]. A 1/d variation was originally believed to characterize the entire PSD range up to 10-20 μm in magnetite [*Parry*, 1965; *Stacey and Banerjee*, 1974], but the data of Robins and Rahman et al. are consistent with a $d^{-0.55}$ dependence of M_{tr} between 1 and 200 μm, and data on large crystals by *Levi* [1974] and Ö. Özdemir (unpublished data, 1996) continue this trend up to millimeter sizes. On the other hand, data on crushed magnetites by *Hartstra* [1983] and D. Dunlop and S. Xu (unpublished data, 1996) are almost size independent above ≈10 μm and support the original notion of a PSD threshold.

The size dependences of weak-field TRM and ARM are very similar: as d^{-1} below 1 μm and $d^{-0.55}$ above 1 μm (Figures 1 and 2). However, the two trends merge smoothly in the case of M_{tr}, whereas they are distinct and nonintersecting in the case of M_{ar}. Internal stress in crushed grains does not seem to influence TRM as much as it does ARM and other room-temperature magnetizations. In part, this may be due to the annealing effect of heating to impart TRM.

TRM/ARM ratios. The ratio of intensities of weak-field TRM and ARM, χ_{tr}/χ_{ar} or Q_t/Q_a, is between 1 and 2 and almost independent of grain size for >1 μm magnetites (Figure 3). (Points GS1-GS6 combine ARM data from *Gillingham and Stacey* [1971] with TRM data for similar-sized grains from *Rahman et al.* [1973].) For >1 μm magnetites, thermal fluctuations and alternating fields are about equally effective in helping moments reverse or walls move.

Below 1 μm, the TRM/ARM ratio rises to values >>1 (Figure 3). Around d= 200 nm, χ_{tr}/χ_{ar} reaches peak values of ≈10 (data of *Levi and Merrill* [1976, 1978]) or ≈20 (samples A1-A3 and D1-D4). In the introduction, we speculated that such contrasting values of χ_{tr} and χ_{ar} might indicate different LEM states carrying TRM and ARM in 100-500 nm magnetites. Whether or not this is the correct explanation, TRM is clearly a much more efficient process than ARM for the same steady field H_o in grains of this size.

Field dependence of ARM and TRM. The contrast between the efficiencies of TRM and ARM magnetizing processes for magnetites in the 200-500 nm size range is clear in Figure 4. TRM intensity M_{tr} is between 5 and almost 20% of saturation remanence M_{rs} in a field H_o of only 1 Oe or 0.1 mT, and the TRM produced by H_o= 17 Oe or 1.7 mT is 45-75% saturated. The corresponding figures for ARM are ≈1% of M_{rs} for a 1 Oe field and 10-15% of saturation when H_o= 17 Oe. Since TRM is completely erased by the 100 mT peak AF used in ARM acquisition [*Dunlop and Argyle*, 1991, Figure 1], none of the difference can be due to a high-coercivity fraction of TRM that is absent from ARM. Either ARM is a remarkably inefficient process or else alternating fields permit grains of this size to transform to a micromagnetic structure whose remanence is low compared to either TRM or saturation remanence. There is some experimental support for this latter idea from domain observations on large titanomagnetite grains, which have few (or occasionally no) walls after TRM acquisition but nucleate additional walls as a result of AF demagnetization [*Halgedahl*, 1991].

It is commonly assumed that M_{tr} and M_{ar} are both proportional to H_o for small inducing fields (1-2 Oe or less). In the case of TRM, this assumed proportionality is built into the Thellier method of determining paleomagnetic field intensity. Figures 5 and 6 test this assumption by plotting the slopes of ARM and TRM induction curves; that is, $\chi_{ar} = dM_{ar}/dH_o$ and $\chi_{tr} = dM_{tr}/dH_o$, as a function of H_o. (The H_o= 1 Oe values of χ_{ar} and χ_{tr} were given in Table 1 and plotted in Figures 1 and 2.) Over any interval in which M_{ar} (or M_{tr}) is linear in H_o, χ_{ar} (or χ_{tr}) should be constant.

Linearity is good in the case of ARM for all magnetites except the smallest (D4, 37 nm), not only in very weak fields but up to the maximum fields used (Figure 5). TRM, on the other hand, is only proportional to H_o in the weak-field region for the two largest magnetites (A2 and A3, 390 and 540 nm). For all the other samples, χ_{tr} changes rapidly between 0 and 2 Oe, by 15-50%, and only becomes approximately constant in much larger fields of 12-17 Oe. In other words, the TRM intensity is most nonlinear in small fields, not large fields.

Theoretical Fits to the TRM and ARM Data

***Néel* [1949] theory.** Nonlinearity of TRM in weak fields and approximate linearity in larger fields is not at all the behavior predicted by *Néel*'s [1949] thermal fluctuation theory of TRM in noninteracting SD grains. Néel's theory leads to the result

$$M_{tr}(H_o) = M_{rs} \tanh[\mu_o V M_s(T_B) H_o / kT_B], \quad (1)$$

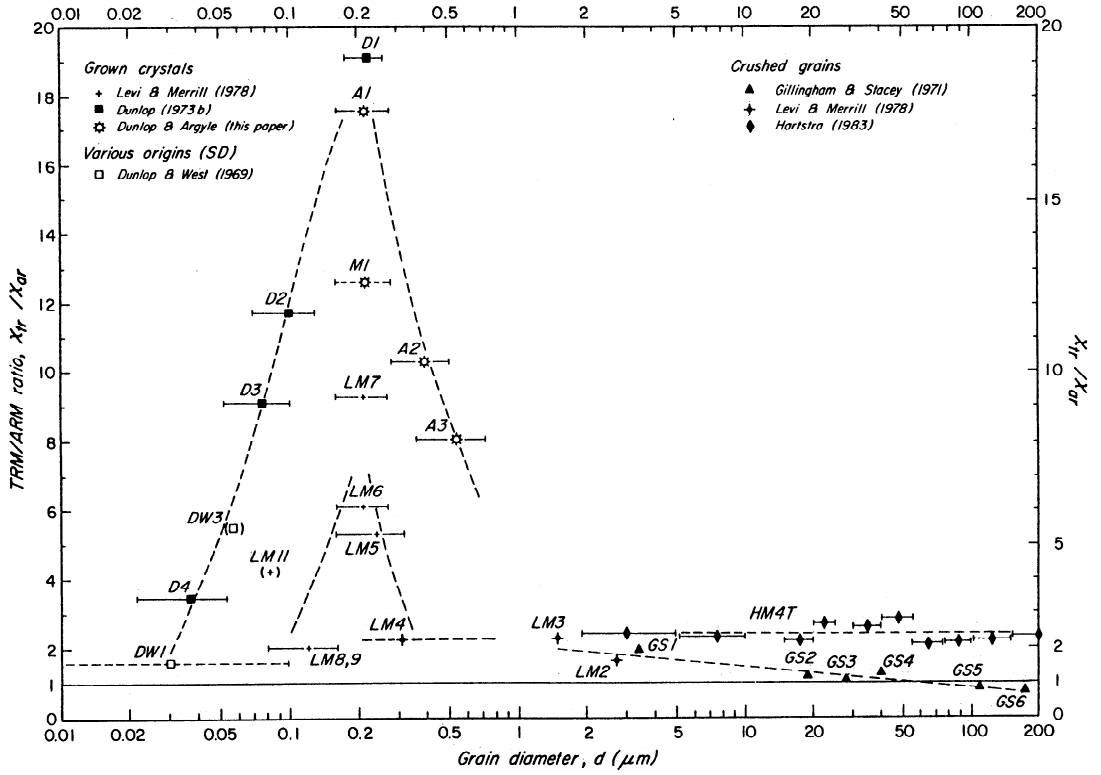

Figure 3. The ratio of weak-field TRM and ARM, χ_{tr}/χ_{ar}, as a function of magnetite grain size d. For d> 1 μm, $\chi_{tr} \approx \chi_{ar}$ for all grain sizes, but for d< 1 μm, $\chi_{tr} >> \chi_{ar}$. The great contrast in TRM and ARM intensities around d= 0.2 μm suggests different TRM and ARM microstates: a low-remanence vortex structure for ARM and a high-remanence two-domain (2D) state for TRM.

in which V is grain volume, M_s is spontaneous magnetization, T_B is blocking temperature (in Kelvins), and k is Boltzmann's constant. The slope $\chi_{tr} = dM_{tr}/dH_o$ of (1) for V corresponding to 37 nm cubes is plotted as the dashed curve in Figure 6. The value of χ_{tr} is predicted to be constant (i.e., $M_{tr} \propto H_o$) for weak fields and to decrease significantly (nonlinear TRM) only when $H_o > 4$ Oe. The very different shapes of theoretical and experimental curves emphasize that Néel SD theory, or other theories based on a tanh TRM function [*Jaep*, 1971; *Stacey and Banerjee*, 1974], are unlikely to explain our TRM data in a satisfying way.

As expected, M_{tr} versus H_o curves predicted by (1) for 37 and 76 nm cubes bear little resemblance to our measured curves (Figure 7). Magnetites larger than 76 nm are not expected to have equilibrium SD structures, but they can exist in metastable SD LEM states [*Boyd et al.*, 1984]. The TRM of such metastable SD grains would saturate in fields of only 1-2 Oe and would be even less like the experimental curves.

There are several lessons to be drawn from Figure 7. First, the experimental curves approach saturation slowly and have approximately the same general aspect for all grain sizes from 37 nm to 540

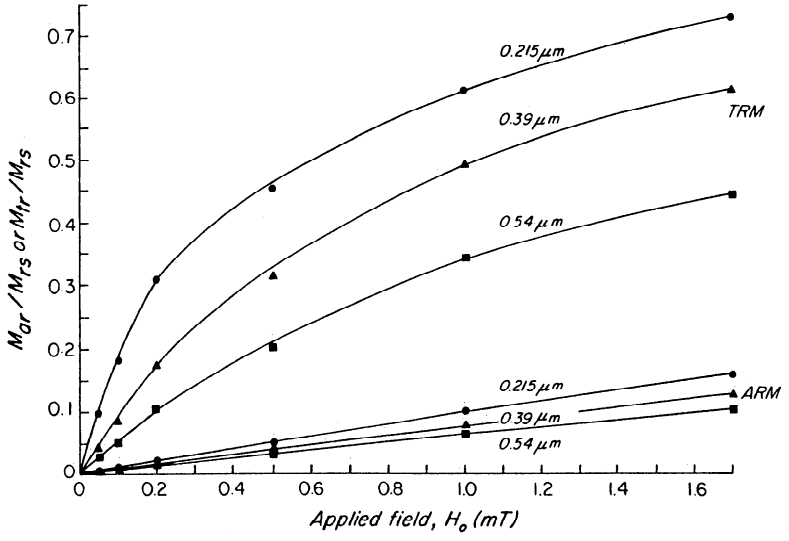

Figure 4. Normalized ARM or TRM, M_{ar}/M_{rs} or M_{tr}/M_{rs}, as a function of DC applied field H_o for samples A1-A3. The rapid initial rise in TRM contrasts with the slow linear change in ARM, and $M_{tr} >> M_{ar}$ for the same H_o.

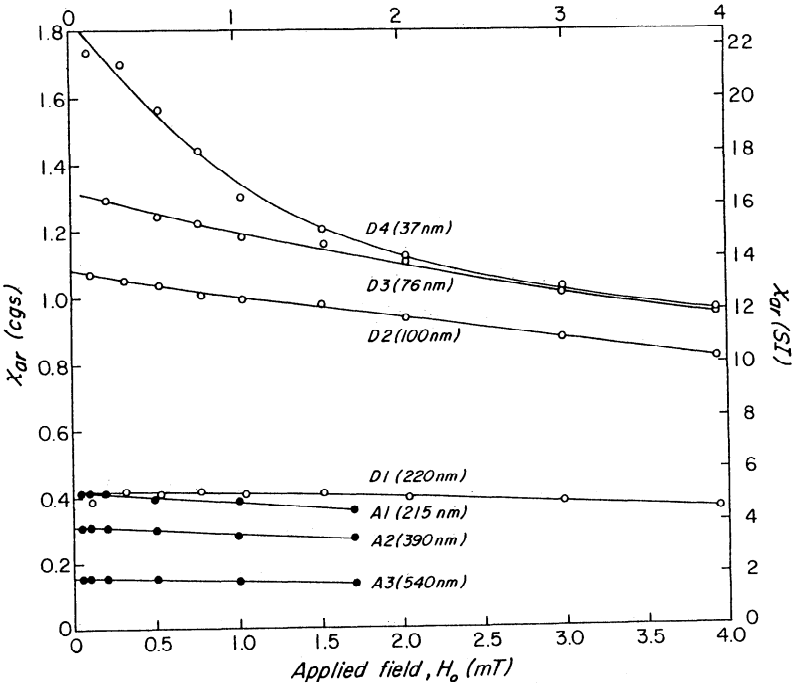

Figure 5. Anhysteretic susceptibility for different values of applied DC field H_o. The constant values of χ_{ar} for most samples indicate that $M_{ar} \propto H_o$.

nm, a range of ≈3000 in total grain volume. If SD-like moments, of vortex structures or domain walls for example, are a source of TRM in these grains, these moments must have similar magnitudes in all cases. They must individually occupy a much smaller fraction of the total volume in the larger grains than in the smaller grains. Second, the persistent linearity of the experimental TRM curves in intermediate and large fields (up to 90 Oe for D1-D4) implies some other, non-SD source of TRM which is difficult to saturate.

Jaep [1969] adapted Néel's theory to produce a kinetic description of ARM. Previous SD ARM models assuming time-independent switching fields had predicted that even a vanishingly small bias field $\mathbf{H}_o$ superimposed on the AF would align all SD moments in the direction of $\mathbf{H}_o$. In other words, χ_{ar} would be infinite. Jaep's model predicted a finite anhysteretic susceptibility, but ARM curves would still rise very steeply, like the theoretical TRM curves of Figure 7. Since experimentally $\chi_{ar} << \chi_{tr}$ (Figures 4-6 and Table 1), this theoretical approach must be abandoned.

***Jaep* [1971] theory.** The interaction field between SD grain moments plays a key role in *Jaep*'s [1971] theory. In simple terms, $\mathbf{H}_o$ must be large enough to overcome the effect of oppositely directed (negative) interaction fields before TRM or ARM can be produced. This has the effect of lowering χ_{tr} and χ_{ar} considerably if grain interactions are stronger than a few Oe. Furthermore, because the interaction field is proportional to grain moment VM_s and $M_s(T)$ decreases as T increases, interactions are less influential at high temperatures. It follows that $\chi_{tr} > \chi_{ar}$, as observed experimentally.

The basic results of Jaep's theory are that

$$p_t = M_{tr}/M_s = \tanh[(\mu_o V M_{sB}/kT_B)(H_o - \lambda_B p_t)] \quad (2)$$

$$p_a = M_{ar}/M_s = \tanh[(\mu_o V M_{so}/kT_o)(\lambda_B/\lambda_o)(H_o - \lambda_o p_a)], \quad (3)$$

$$\lambda_B/\lambda_o = (M_{sB}/M_{so})(T_o/T_B)^{1/2}. \quad (4)$$

In (2)-(4), λp represents an interaction field, subscripts o and B referring to room-temperature T_o and the blocking temperature T_B, respectively. The fraction p_t (or p_a) of SD grains with moments parallel to $\mathbf{H}_o$ is measured as the fractional magnetization M_{tr}/M_s (or M_{ar}/M_s). Jaep assumed an aligned assembly of uniaxial grains; an isotropic assembly would have $p = M/M_{rs}$. Note that p_t is frozen in at T_B and does not change in cooling to T_o.

Jaep's results constitute a mean-field approach to interactions. Every grain experiences the same interaction field, $\lambda_B p$ at T_B or $\lambda_o p$ at T_o, when the assembly of grains has net magnetization p. This

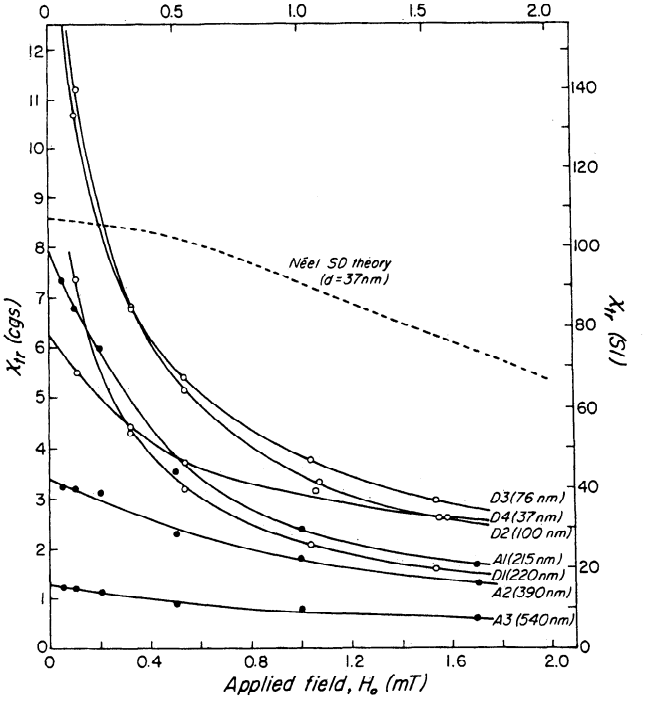

Figure 6. Thermoremanent susceptibility for different applied fields. Particularly in weak fields, χ_{tr} varies strongly for most samples, violating the assumption $M_{tr} \propto H_o$ in Thellier paleointensity determination.

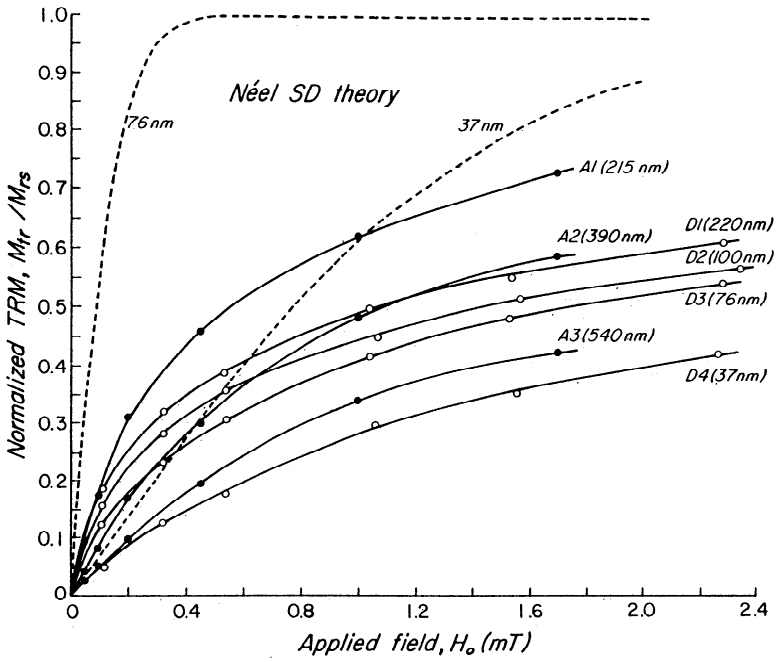

Figure 7. Experimental TRM acquisition curves for the A and D series magnetites compared to the predictions of *Néel*'s [1949] theory of noninteracting SD grains. The theory cannot explain the rapid initial rise of the experimental curves combined with their gradual approach to saturation.

rather unrealistic assumption is very limiting in trying to explain real data (Figure 8). Increasing the interaction strength λ_B merely "shears" the original Néel tanh TRM function (the λ_B=0 curve) to the right, in the same manner that the internal demagnetizing field shears the hysteresis loop of a multidomain grain [*Néel*, 1955], without changing its basic form. Figures 6 and 7 show that none of the experimental TRM curves resembles a tanh function. Therefore it is not surprising that no single value of λ_B produces even an approximate fit between Jaep's theory and our data (Figure 8). In the example shown, λ_B must be varied from 0 for small H_o to 100 for large H_o in order to match individual M_{tr} values, implying a distribution of interaction fields from 0 to $\lambda_B p_t \approx 100 \times 0.7 = 70$ Oe.

ARM model curves are given approximately by the TRM model curves with a scaled-up λ. Quite linear functions can be produced in this way, but very high values of mean interaction field are required to explain the low values of χ_{ar} that we observe.

***Dunlop and West* [1969] theory.** A distribution of interaction fields, which takes account of variations in the spacing and orientation of SD grains, is the central feature of the *Dunlop and West* [1969] theory. This is a local-field model, in which a grain can reverse its moment and acquire TRM or ARM only when H_o exceeds the local value of interaction field at that grain. The distribution function $f(\lambda)d\lambda$ is determined from isothermal remanence measurements via the Preisach diagram [*Dunlop et al.*, 1990]. Thus $f(\lambda)d\lambda$ is not arbitrarily calculated to give best fit to ARM or TRM curves but is measured independently of any ARM or TRM data.

The basic results of the Dunlop and West theory are that

$$p_t = M_{tr}/M_{rs} = \int_0^{H_o} f(\lambda_B)d\lambda_B \quad (5)$$

$$p_a = M_{ar}/M_{rs} = \int_0^{H_o} f(\lambda_o)d\lambda_o \quad (6)$$

$$\lambda_B/\lambda_o = (M_{sB}/M_{so}). \quad (7)$$

Equations (5)-(7) produce a good first-order fit to the ARM data of the D series samples but are only a slight improvement on the single-λ Jaep theory in fitting the TRM data (Figure 9). The theoretical curves rise slowly at small fields, giving lower than observed initial χ_{tr} values, but saturate too rapidly. Furthermore, to produce even an average fit, we had to assume blocking temperatures T_B= 460°C for D4 (37 nm) and 540°C for D1 and D3 (220 and 76 nm). These are 15°-25°C lower than measured average unblocking temperatures for D1 and D3 [*Dunlop*, 1973b]. Using higher values for T_B caused a steeper initial rise, although predicted χ_{tr} values were still lower than measured ones, but saturation occurred at unrealistically small fields.

***Néel* [1955] theory.** In view of the unpromising fits of Figure 9, modeling in terms of interacting SD moments was not attempted for

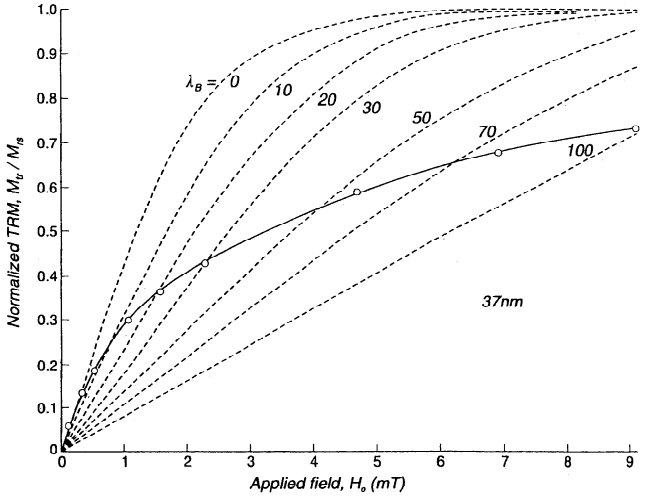

Figure 8. Measured TRM for sample D4 (<d>= 37 nm) compared to the predictions of the *Jaep* [1971] mean-field interaction theory. There is no correspondence between the shapes of experimental and theoretical curves. In order to match individual data points, the interaction coefficient λ_B must change from 0 to 100.

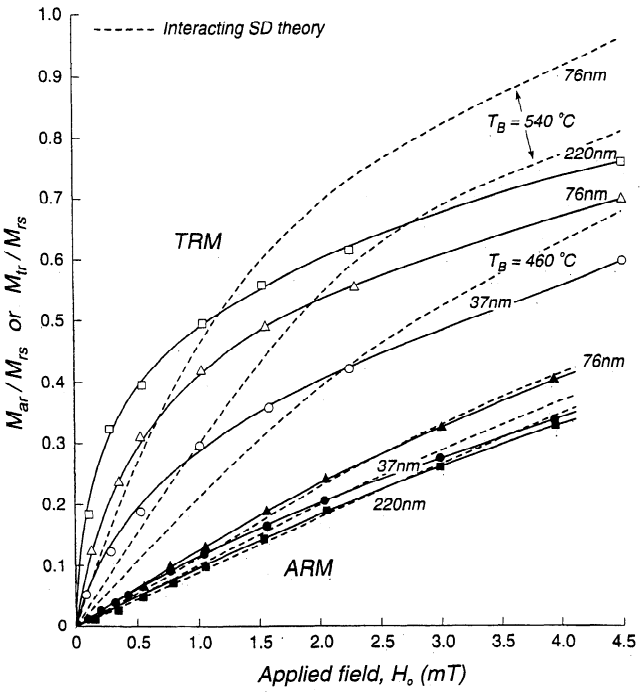

Figure 9. Measured TRMs and ARMs for D series samples compared to the predictions of the *Dunlop and West* [1969] local-field interaction theory. The ARM curves are well accounted for, but extrapolating the measured room-temperature interaction distribution f(λ) to T_B produces a mediocre fit to the TRM data.

the A series magnetites, which in any case are well above critical SD size. The M_{rs}/M_s ratios of A1-A3 range from 0.06-0.09 [*Argyle and Dunlop*, 1990]. These are much below SD values, but they are rather high for vortex or other circular spin structures. They would be compatible with domain wall or double vortex moments. In addition, the very high χ_{tr}/χ_{ar} ratios of these magnetites imply that following TRM the grains could be in higher-remanence LEM states, 2D for example, even if they adopt a low-remanence vortex or similar state following ARM or AF demagnetization. For these reasons, we modeled the TRM data of A1-A3 using *Néel*'s [1955] 2D theory.

According to *Néel* [1955], a domain wall which has been displaced by $\mathbf{H}_o$ will reequilibrate its position at each new temperature during cooling under the joint influence of the internal demagnetizing field and local potential wells representing the pinning effect of crystal defects. Both the demagnetizing field and the barriers between wells grow as T decreases, but at T_B the potential barriers begin to grow more rapidly than self-demagnetization, and the wall is trapped. The basic results of the theory [*Dunlop and Waddington*, 1975; *Day*, 1977; *Dunlop and Xu*, 1994] are that

$$M_{tr} = m(m\text{-}1)^{1\text{-}1/m} N^{-1} H_{co}^{\ 1/m} H_o^{\ 1\text{-}1/m}$$

$$= 2N^{-1} H_{co}^{\ ½} H_o^{\ ½} \qquad \text{if } m=2 \qquad (8)$$

where

$$H_c(T)/H_{co} = [M_s(T)/M_{so}]^m. \qquad (9)$$

Equation (8) predicts absolute TRM intensity, unlike equations (1), (2) and (5) which predict TRM as a fraction of saturation remanence, that is, the fractional alignment p_t of SD moments.

Fits of (9) to coercive force data from 305°-525°C [from *Argyle and Dunlop*, 1990] gave m values of 1.45 and 1.60 for samples A3 and A2. The fit was poorer for sample A1. However, the best fit of (8) to the experimental TRM data for A1-A3 resulted from using Néel's suggested value m=2 (Figure 10). For fields ≥0.2 mT, the predicted M_{tr} values are reasonably close to measured values, and the theoretical and experimental curves have similar shapes.

In the weak-field region below 0.2 mT, paleomagnetically the most interesting region, the quadratic theoretical curves rise too steeply (unlike SD theoretical fits, which all had too shallow initial slopes) and predict χ_{tr} values that are 2-4 times too high. This failure is not surprising. *Néel* [1955] noted that when H_o is small, thermal fluctuations would unblock domain walls below the blocking temperature predicted from wall pinning alone and M_{tr} should be proportional to H_o. Unfortunately, Néel's thermal fluctuation theory of wall blocking contains parameters which are experimentally inaccessible. Thus we cannot compare its predictions to our data.

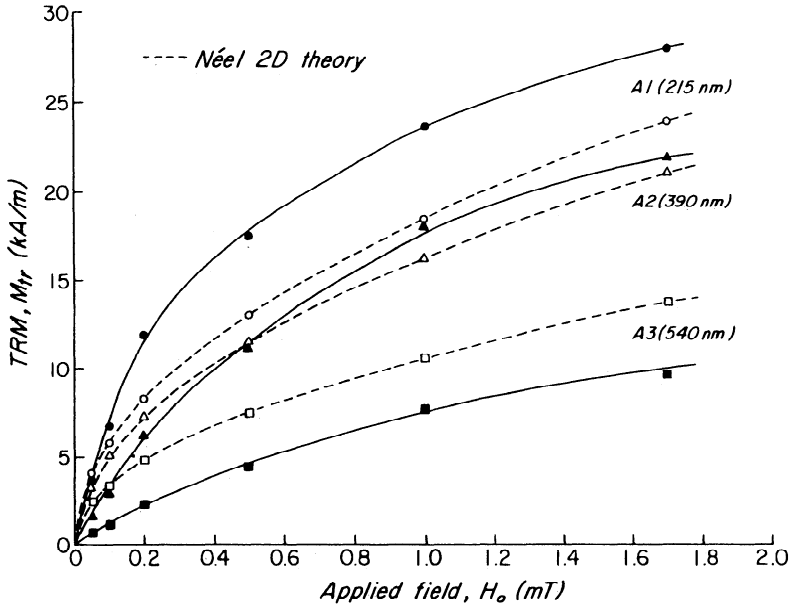

Figure 10. Experimental TRM data for A series samples compared to the predictions of the *Néel* [1955] theory of wall pinning in 2D grains. For moderate and strong fields, the theory explains both the aspect and numerical values of the TRM curves.

Pseudo-single-domain theory. If magnetites in the 200-500 nm size range do adopt 2D or analogous states when they acquire TRM, there are potentially two independent sources of remanence. In the last section, we dealt with pinned displacements of the wall in each grain, which can account for TRM in moderate and strong fields (Figure 10). But the wall itself has a moment, given by $(2/\pi)AtM_s$ (A and t are wall area and thickness, respectively) if spins rotate uniformly across a Bloch wall [*Stacey and Banerjee*, 1974]. The wall moment has two opposite orientations, depending on the sense of spin rotation, between which it can reverse. In either orientation, the wall moment is perpendicular to and independent of M_{tr} due to wall displacement. Thus the wall moment (called a "psark" by *Dunlop* [1977]) has the properties of a SD moment embedded in a multidomain matrix.

Domain wall moments and moments associated with surface terminations of walls (e.g., spikes, closure domains [see *Özdemir et al.*, 1995]) are promising candidates for explaining the PSD 1/d size dependence of weak-field TRM (and ARM) evident in Figures 1 and 2. This is because both depend on area, either of the domain wall or of the grain surface, leading to a moment per unit volume $\propto$ A/V or 1/d.

The experimental TRM curves (Figure 7) are strikingly similar in shape over a broad range of grain volumes, especially for fields $H_o \geq$ 0.4 mT. This similarity contrasts with the very size-dependent theoretical curves which would result if entire grains acted in SD fashion (metastable SD states), but is consistent with domain wall moments as the source of PSD behavior in this size range.

Dunlop et al. [1974] were successful in explaining the TRM curves of D1-D4 by fitting to a PSD relation

$$M_{tr} = AH_o + Bf(\alpha H_o). \quad (10)$$

The term AH_o represents wall displacement TRM and is based on *Stacey*'s [1958] expression

$$M_{tr} = N^{-1}(1+N\chi_i)^{-1}(M_{so}/M_{sB})H_o, \quad (11)$$

in which χ_i is intrinsic susceptibility due to the internal field, which can be considerably larger than externally observed susceptibility χ_o. The self-demagnetization or screening factor $(1+N\chi_i)^{-1}$ is problematic because walls in 2D grains have less freedom of adjustment when $H_o \to 0$ than in large grains with many walls. For the wall moment term $Bf(\alpha H_o)$, Dunlop et al. used a function suggested by *Stacey and Banerjee* [1974],

$$Bf(\alpha H_o) = n\mu_{max} \int_0^1 \int_0^1 xy \tanh(\alpha\mu_o H_o xy)\, dx\, dy \quad (12)$$

$$\alpha = (\mu_{max}/kT_B)(M_{sB}/M_{so}), \quad (13)$$

which averages *Néel*'s [1949] SD equation (1) over all angles and over a uniform distribution of PSD moments (n per unit volume) from 0 to μ_{max}.

We propose for ARM a relation analogous to (10):

$$M_{ar} = A'H_o + B'f(\alpha' H_o). \quad (14)$$

Assuming that the AF plays the same role at T_o that thermal energy does at T_B, we can obtain A′ from A and α′ from α by replacing T_B in (13) by T_o and omitting (M_{so}/M_{sB}) or its inverse in (11) and (13).

The MD+PSD curve fits were quite successful for both samples A1-A3 (Figure 11) and D1-D4 (not shown). The nonlinear or PSD term $Bf(\alpha H_o)$ causes a rapid initial rise in TRM, thus explaining the high observed initial χ_{tr} values. This term saturates beyond the weak-field region and the linear or multidomain term AH_o determines χ_{tr} in higher fields. The poorest fit to the TRM data is for intermediate fields around 0.5 mT or 5 Oe. The ARM curves are very nearly linear for most samples, and the PSD term $B'f(\alpha' H_o)$ plays a minor role in the curve fits. Curve fit parameters for all samples are given in Tables 2 and 3.

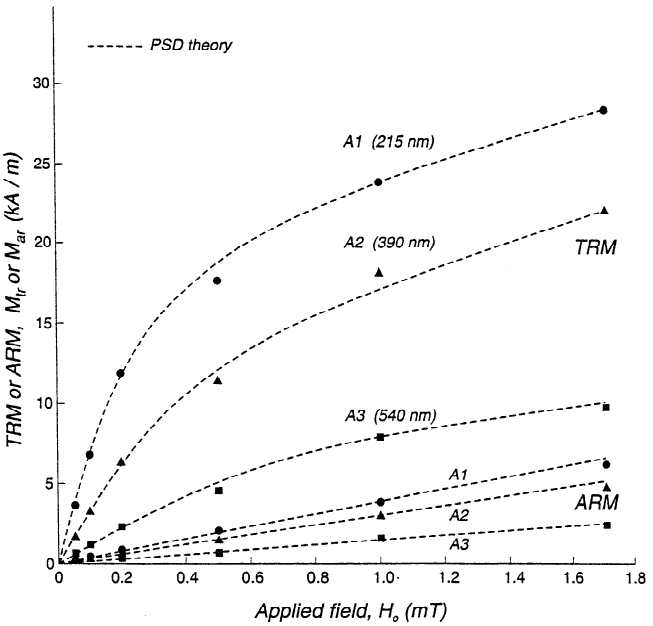

Figure 11. Experimental TRM and ARM data for A series samples compared to the predictions of a PSD theory combining MD and SD-like contributions to TRM. By varying the parameters, excellent fits are obtained in both weak- and moderate-field regions.

From the curve fit parameters α (or α′) and B (or B′), we calculated the maximum PSD moment μ_{max}, using (13) or its equivalent for ARM, and the numbers n or n′ of PSD moments per unit volume, from $n = B/\mu_{max}$ or the equivalent relation for ARM. The number of moments per grain follows from n or n′. These calculated properties are listed in Tables 2 and 3.

In the case of TRM, μ_{max} is comparable to the SD moment μ_{SD} for magnetites D2-D4, which are close to critical SD size, but μ_{max} is more or less constant and $<<\mu_{SD}$ in the larger magnetites (Table 2). In the case of ARM, μ_{max} is an order of magnitude smaller than for TRM (Table 3), implying that TRM and ARM have their sources in different microstates. The calculated number of PSD moments per grain is about one for magnetites near SD size whether they carry TRM or ARM. In larger magnetites, from $\approx$2 to $\approx$20 moments per grain contribute to TRM, but there is a negligible PSD contribution to ARM.

Discussion

Initial susceptibility χ_o and weak-field ARM M_{ar} or ARM susceptibility χ_{ar} are widely used to normalize depositional remanence (DRM) intensities in sediment paleointensity studies. Our measurements confirm that χ_o is a suitable normalizing factor in the case of submicron magnetites with low internal stresses. The value of χ_o is then almost independent of grain size and mainly measures magnetite concentration. Of course, our magnetites are not representative of all the magnetic material in sediment cores. Ocean Drilling Program cores in particular may contain coarser wind-blown or ice-rafted magnetites which, if they have been abraded in desert environments or otherwise strained, could be analogous to highly

Table 2. TRM Curve-Fit Parameters and Calculated Properties

Sample	<d>, nm	<T_B>, K	M_{sB}/M_{so}	A, emu/cm³ Oe	B, emu/cm³	α, Oe^{-1}	μ_{SD}, 10^{-13} emu	μ_{max}, 10^{-13} emu	n, 10^{14} cm^{-3}	Number per Grain
A3	540	842	0.14	0.20	30	0.3	760	2.5	1.20	≈20
A2	390	840	0.17	0.60	50	0.5	290	3.4	1.45	≈10
A1	215	838	0.20	0.60	75	0.8	48	4.6	1.65	≈2
D1	220	838	0.20	0.45	75	0.7	52	4.1	1.85	≈2
D2	100	833	0.24	0.60	125	0.6	4.9	2.9	4.35	≈0.5
D3	76	828	0.26	0.75	140	0.5	2.1	2.1	6.55	≈0.33
D4	60*	820*	0.33*	0.90	110	0.3	1.0	1.0	10.6	≈0.25

*T_B and M_{sB}/M_{so} corresponding to the maximum grain size were used in calculations.

stressed crushed or glass-ceramic magnetites. Biogenic magnetites are closer analogs of the fine-grained hydrothermal magnetites we have studied, but although they may dominate the stable natural remanent magnetization (NRM) of a sediment, they do not necessarily dominate the susceptibility.

ARM is less suitable than χ_o as a normalizing factor because of its dependence on grain size, which is even stronger than that of saturation remanence (SIRM), M_{rs}, when d<1 μm. On the other hand, if detecting grain size variations is the objective, χ_{ar} is the most suitable of the parameters. In the method proposed by *King et al.* [1982, 1983], χ_{ar} and χ_o are used jointly to monitor both grain size and concentration variations in sediment cores. Our detailed data for χ_{ar} in the 0.2-0.5 μm range could be used to refine King et al.'s nomograms. However, such refinement will not help in selecting reliable sediments for relative paleointensity determinations because only magnetite grain sizes >1 μm have sufficiently similar ARM and DRM size dependences to be useful [cf. *King et al.*, 1983].

The grain size dependence of χ_{tr} is very similar to that of χ_{ar}: as d^{-1} when d<1 μm and as $d^{-0.55}$ or as $d^{-0.27}$ or weaker, depending on the data set examined, when d>1 μm. This similarity argues for a common PSD mechanism governing the size dependences of ARM and TRM. However, the ARM and TRM microstates must be rather different in <1 μm grains. The efficiencies of the ARM and TRM processes, as measured by χ_{ar} and χ_{tr}, are similar in grains larger than 1 μm but very different in smaller grains (Table 1 and Figure 3). Now $Q_a \approx 1$ for d≥ 0.2 μm, showing that initial susceptibility (which was measured from an AF demagnetized state) and ARM processes have similar efficiencies, but Q_t ranges from 3 to 27 over the size span 215-540 nm (Table 1). The implication is that TRM resides in high-remanence, probably metastable, microstates in this size range. On the basis of predictions of micromagnetic models [*Williams and Dunlop*, 1989, 1995; *Newell et al.*, 1993; *Fabian et al.*, 1996; *Fukuma and Dunlop*, 1997], these microstates are likely two- or three-domain or double-vortex for TRM and single-vortex for ARM or following AF demagnetization.

ARM and TRM intensities increase with applied field H_o in similar ways in moderate and strong fields, but in very different ways in the weak-field (≤0.2 mT) region (Figures 4 and 9). The steep initial rise of the M_{tr}-H_o curves is totally lacking in the M_{ar}-H_o curves. High initial χ_{tr} is most pronounced for grains around 0.2 μm in size (Figure 7) and causes a peak in χ_{tr}/χ_{ar} (Figure 3). Beyond the weak-field region, the M_{tr}-H_o curves have a slow approach to saturation which is similar for all grain sizes. These observations guided our theoretical modeling of the data.

Most of our samples have very nonlinear M_{tr}-H_o curves (i.e., nonconstant χ_{tr}) in weak fields (Figure 6), quite unlike the linear behavior assumed in Thellier paleointensity determination. Thus it is important to use a laboratory field more or less equal to the paleofield in paleointensity work; a suitable field strength could be chosen from experiments on pilot specimens.

Noninteracting SD theory [*Néel*, 1949] was unsuccessful in explaining the TRM data of even the finer magnetites (D series). The Néel curves, which are linear in small fields, rapidly saturating, and very grain size dependent, are totally unlike the nonlinear, slowly saturating, and weakly size dependent experimental curves (Figure 7). The addition of grain interactions with strength λ (mean-field theory [*Jaep*, 1971]) did not improve matters (Figure 8). Interactions with a distribution f(λ) determined from room-temperature Preisach analysis (local-field theory [*Dunlop and West*, 1969]) gave a good fit to the ARM data for D1-D4 but a poor fit to the TRM data. Extrapolating f(λ) to high temperatures is not satisfactory for these magnetites.

In theory, the ratio between weak-field TRM and ARM in either interaction theory is approximately λ_o/λ_B, which according to *Jaep*'s [1971] theory (equation (4)) is $(M_{so}/M_{sB})(T_B/T_o)^{1/2}$ and according to *Dunlop and West*'s [1969] theory (equation (7)) is M_{so}/M_{sB}. Using the <T_B> and M_{sB}/M_{so} values in Table 2, Dunlop and West's theory predicts χ_{tr}/χ_{ar} ratios of 3-7, while Jaep's theory predicts values of 5-12 (Table 4). The experimental TRM/ARM ratios range from 3.45 to 19.2. The closest agreement is actually for the largest magnetites, which are the least appropriate for any SD theory. There is also a practical difficulty in using either theory as the basis of an ARM analog method of paleointensity determination: the theoretical ratios are very sensitive to the exact value of <T_B>, and this temperature cannot usually be determined to better than ±10°C.

Néel's [1955] theory of TRM due to wall displacement in a two-domain grain gave a good average fit to absolute M_{tr} values of samples A1-A3 (215-540 nm) for fields >0.2 mT (Figure 10). The shapes of experimental and theoretical curves match so well that Néel's picture of walls (or some equivalent structure) reequilibrating continuously during cooling in response to self-demagnetization must be basically correct in the moderate- and strong-field region. No other mechanism can plausibly explain why TRM saturates so slowly. Grain interaction fields are unlikely to exceed 10 mT or so, but the internal demagnetizing field can be as large as several hundred mT in the approach to saturation.

TRM acquired in weak fields comparable to the geomagnetic field is not well explained by the *Néel* [1955] theory (Figure 10). We had good success in fitting the TRM and also the ARM data by a sum of SD-like and MD-like terms (equations (10)-(14) and Figure 11). The SD-like term, which averages a tanh function over all orientations and magnitudes of PSD moments, saturates rapidly and explains the weak-field TRM. The MD-like term, linear in H_o and modeled on *Stacey*'s [1958] theory of large grains with many walls, scarcely contributes to weak-field TRM but explains the slow rise to saturation in strong fields. Of course, by using two adjustable parameters, one would expect to achieve better curve fits; indeed, the fits in Figure 10 are convincing precisely because the parameter

Table 3. ARM Curve-Fit Parameters and Calculated Properties

Sample	<d>, nm	A′, emu/cm³ Oe	B′, emu/cm³	α′, Oe^{-1}	μ_{SD}, 10^{-13} emu	μ_{max}, 10^{-13} emu	n′, 10^{14} cm^{-3}	Number per Grain
A3	540	0.15	0	-	760	-	0	0
A2	390	0.30	0	-	290	-	0	0
A1	215	0.40	0	-	48	-	0	0
D1	220	0.40	0	-	52	-	0	0
D2	100	0.80	10	0.30	4.9	0.12	8.4	≈1
D3	76	0.95	12	0.30	2.1	0.12	10.0	≈0.5
D4	60*	0.90	20	0.35	1.0	0.14	14.3	≈0.3

*Maximum grain size was used in calculations.

Table 4. Values of $R = \chi_{tr}/\chi_{ar}$ Observed for the Experimental Samples Compared to Values Predicted by the Theories of *Dunlop and West* [1969], $R_{DW} = M_{so}/M_{sB}$, and *Jaep* [1971], $R_J = (M_{so}/M_{sB})(T_B/T_o)^{1/2}$

Sample	<d>, nm	R_{DW}	R_J	R_{obs}
A3	540	7.1	12.1	8.0
A2	390	5.9	10.0	10.3
A1	215	5.0	8.5	17.6
D1	220	5.0	8.5	19.2
D2	100	4.2	7.0	11.7
D3	76	3.8	6.5	9.1
D4	*60	3.0	5.1	3.45

*T_B and M_{sB}/M_{so} corresponding to the maximum grain size were used in calculations.

m in Néel's theory was not adjusted. On the other hand, if the basic idea of two independent sources of TRM (and ARM) is correct, the curve fit parameters give valuable information about the properties of these sources.

Comparing equations (10) and (11), we have that $A = N^{-1}(1+N\chi_i)^{-1}(M_{so}/M_{sB})$. For a two-domain grain, N varies from about 1.6 to 2.0 (cgs) depending on the wall displacement [*Dunlop*, 1983]. *Heider et al.* [1996] calculate χ_i values ranging from about 1 to 100 (cgs) as grain size varies from 0.75 μm to 1 mm. The lower limit gives a screening factor $(1+N\chi_i)^{-1} \approx 1/3$. From Table 2, M_{so}/M_{sB} varies from 3 to 7 for our samples. Thus we would expect A to be in the range 0.5-1.5. All but one of our samples have experimental values of A between 0.45 and 0.9, so the MD model used seems reasonable for TRM. However, it is not so reasonable for the ARM data. A′ should be a factor $M_{sB}/M_{so} = 1/3$ to 1/7 smaller than A, in the range 0.1-0.5, but experimentally the values of A′ and A are quite similar (Tables 2 and 3). Thus a two-domain state seems to be inappropriate for ARM, as we have concluded earlier on other grounds.

Turning to the SD-like weak-field TRM, the maximum PSD moment μ_{max} calculated from the TRM data of samples D2-D4, whose grains are close to SD size, is very nearly equal to μ_{SD}. When $d \geq 0.1$ μm, μ_{max} is almost constant at $(2.5\text{-}4.6) \times 10^{-13}$ cmu. Such a PSD moment is about 10% of μ_{SD} in 0.2 μm grains, and ≈2 such moments are predicted per grain. Given the rough nature of the calculations, this result is consistent with moments of domain walls in two- or three-domain grains being the TRM carrier. However, in 390 and 540 nm grains (A2 and A3), μ_{max} is ≤1% of μ_{SD}, and 10-20 such moments are predicted per particle. Sections of walls, perhaps individual linked vortices, seem to act independently in acquiring TRM in these larger grains.

The SD-like contribution to ARM is so small that no meaningful estimates of μ_{max} or the number of moments per grain could be calculated except for the quasi-SD magnetites D2-D4. Interestingly enough, the number of moments per grain is about 0.3-1, as for TRM, but $\mu_{max} << \mu_{SD}$. These results are consistent with low-remanence single-vortex ARM microstates, a conclusion we reached earlier from other evidence.

Conclusions

1. Initial susceptibility χ_o is weakly dependent on grain size and somewhat more strongly dependent on grain shape in 0.1-0.5 μm magnetites. In this size range, χ_o is the best normalizing parameter to correct measured remanences for magnetite concentration, in sediment cores containing fine-grained low-stress magnetites for example.

2. Anhysteretic susceptibility χ_{ar} is strongly dependent on grain size, varying approximately as d^{-1} in 0.1-0.5 μm magnetites, and is an excellent parameter to use, in conjunction with χ_o, to monitor grain size variations in sediment or other samples.

3. Thermoremanent susceptibility χ_{tr} depends strongly on grain size, also as d^{-1}, in 0.1-0.5 μm magnetites. This similarity argues for some common source of the PSD size dependences of ARM and TRM.

4. However, the microstates responsible for ARM and TRM seem to be different in submicron magnetites. The most striking evidence is a pronounced peak in χ_{tr}/χ_{ar} around 0.2 μm. ARM and TRM have similar intensities in >1 μm magnetites, but TRM is as much as 20 times more intense than ARM in <1 μm magnetites.

5. The main difference between TRM and ARM acquisition curves is a rapid rise in TRM in fields ≤0.2 mT compared to a slow rise in ARM. In larger fields, TRM and ARM have similar slow approaches to saturation.

6. TRM is very nonlinear in fields ≤0.2 mT for most of our samples, contrary to the assumptions of Thellier and most other paleointensity determination methods.

7. Single-domain theories, with or without interactions, cannot explain the rapid initial rise but slow saturation of experimental TRM curves for 0.1-0.5 μm magnetites. Nevertheless, the χ_{tr}/χ_{ar} ratio is correctly predicted within a factor 2-3 by interaction theories of TRM and ARM.

8. *Néel*'s [1955] two-domain theory accounts for the slow rise of TRM curves in moderate and strong fields. The agreement of theory and experiment, obtained without curve fitting, is evidence for the existence of walls in the TRM microstates of 0.2-0.5 μm magnetites.

9. Only a PSD combination of SD-like and MD-like carriers can explain both weak-field and strong-field TRM and ARM.

10. The MD curve-fit parameter is consistent with predictions for two-domain grains of submicron size in the case of TRM, but not in the case of ARM.

11. The SD-like curve-fit parameters give numbers and magnitudes of PSD moments that are consistent with entire SD grains carrying weak-field TRM when d≤ 0.1 μm, moments of walls in two- or three-domain structures carrying TRM when d≈ 0.2 μm, and moments of wall segments (10-20 per grain) carrying TRM when d= 0.4-0.55 μm.

12. In contrast to TRM, the SD-like contribution to ARM is very small, even for weak fields. Where it can be calculated with reasonable confidence, each grain has approximately one such moment, but its magnitude is only 2-4% of the SD moment (D3 and D2, d= 76 and 100 nm). The ARM microstate in these grains is probably a single-vortex structure.

Acknowledgments. We thank Randy Enkin, Paul Johnson, and an anonymous referee for helpful reviews. This research has been supported by the Natural Sciences and Engineering Research Council of Canada through grant A7709 to D.J.D.

References

Argyle, K. S., and D. J. Dunlop, Low-temperature and high-temperature hysteresis of small multidomain magnetites (215-540 nm), *J. Geophys. Res.*, *95*, 7069-7083, 1990.

Bailey, M. E., and D. J. Dunlop, On the use of anhysteretic remanent magnetization in paleointensity determination, *Phys. Earth Planet. Inter.*, *13*, 360-362, 1977.

Banerjee, S. K., and J. P. Mellema, A new method for the determination of paleointensity from the A.R.M. properties of rocks, *Earth Planet. Sci. Lett.*, *23*, 177-184, 1974.

Boyd, J. R., M. Fuller, and S. L. Halgedahl, Domain wall nucleation as a controlling factor in the behaviour of fine magnetic particles in rocks, *Geophys. Res. Lett.*, *11*, 193-196, 1984.

Dankers, P. H. M., Magnetic properties of dispersed natural iron oxides of known grain size, Ph.D. thesis, Univ. of Utrecht, Netherlands, 1978.

Day, R., TRM and its variation with grain size, *J. Geomagn. Geoelectr., 29*, 233-265, 1977.

Dunlop, D. J., Superparamagnetic and single-domain threshold sizes in magnetite, *J. Geophys. Res., 78*, 1780-1793, 1973a.

Dunlop, D. J., Thermoremanent magnetization in submicroscopic magnetite, *J. Geophys. Res., 78*, 7602-7613, 1973b.

Dunlop, D. J., The hunting of the 'psark', *J. Geomagn. Geoelectr., 29*, 293-318, 1977.

Dunlop, D. J., On the demagnetizing energy and demagnetizing factor of a multidomain ferromagnetic cube, *Geophys. Res. Lett., 10*, 79-82, 1983.

Dunlop, D. J., Hysteresis properties of magnetite and their dependence on particle size: A test of pseudo-single-domain remanence models, *J. Geophys. Res., 91*, 9569-9584, 1986.

Dunlop, D. J., and K. S. Argyle, Separating multidomain and single-domain-like remanences in pseudo-single-domain magnetites (215-540 nm) by low-temperature demagnetization, *J. Geophys. Res., 96*, 2007-2017, 1991.

Dunlop, D. J., and E. D. Waddington, The field dependence of thermoremanent magnetization in igneous rocks, *Earth Planet. Sci. Lett., 25*, 11-25, 1975.

Dunlop, D. J., and G. F. West, An experimental evaluation of single domain theories, *Rev. Geophys., 7*, 709-757, 1969.

Dunlop, D. J., and S. Xu, A comparison of methods of granulometry and domain structure determination (abstract), *Eos Trans. AGU, 74*, Fall Meet. Suppl., 203, 1993.

Dunlop, D. J., and S. Xu, Theory of partial thermoremanent magnetization in multidomain grains, 1, Repeated identical barriers to wall motion (single microcoercivity), *J. Geophys. Res., 99*, 9005-9023, 1994.

Dunlop, D. J., J. A. Hanes, and K. L. Buchan, Indices of multidomain magnetic behaviour in basic igneous rocks: Alternating-field demagnetization, hysteresis, and oxide petrology, *J. Geophys. Res., 78*, 1387-1393, 1973.

Dunlop, D. J., F. D. Stacey, and D. E. W. Gillingham, The origin of thermoremanent magnetization: Contribution of pseudo-single-domain magnetic moments, *Earth Planet. Sci. Lett., 21*, 288-294, 1974.

Dunlop, D. J., M. E. Bailey, and M. F. Westcott-Lewis, Lunar paleointensity determination using anhysteretic remanence (ARM): A critique, *Geochim. Cosmochim. Acta, 39*, suppl. 6, 3063-3069, 1975.

Dunlop, D. J., M. F. Westcott-Lewis, and M. E. Bailey, Preisach diagrams and anhysteresis: Do they measure interactions? *Phys. Earth Planet. Inter., 65*, 62-77, 1990.

Enkin, R. J., and W. Williams, Three-dimensional micromagnetic analysis of stability in fine magnetic grains, *J. Geophys. Res., 99*, 611-618, 1994.

Fabian, K., A. Kirchner, W. Williams, F. Heider, A. Hubert, and T. Leibl, Three-dimensional micromagnetic calculations for magnetite using FFT, *Geophys. J. Int., 124*, 89-104, 1996.

Fukuma, K., and D. J. Dunlop, Grain size dependence of two-dimensional micromagnetic structures for pseudo-single-domain magnetite (0.2-2.5 μm) *Geophys. J. Int.*, in press, 1997.

Gillingham, D. E. W., and F. D. Stacey, Anhysteretic remanent magnetization (A.R.M.) in magnetite grains, *Pure Appl. Geophys., 91*, 160-165, 1971.

Halgedahl, S. L., Magnetic domain patterns observed on synthetic Ti-rich titanomagnetites as a function of temperature and in states of thermoremanent magnetization, *J. Geophys. Res., 96*, 3943-3972, 1991.

Hartstra, R. L., A comparative study of the ARM and I_{sr} of some natural magnetites of MD and PSD grain size, *Geophys. J. R. Astron. Soc., 71*, 497-518, 1982.

Hartstra, R. L., TRM, ARM and Isr of two natural magnetites of MD and PSD grain size, *Geophys. J. R. Astron. Soc., 73*, 719-737, 1983.

Heider, F., D. J. Dunlop, and N. Sugiura, Magnetic properties of hydrothermally recrystalized magnetite crystals, *Science, 236*, 1287-1290, 1987.

Heider, F., A. Zitzelsberger, and K. Fabian, Magnetic susceptibility and remanent coercive force in grown magnetite crystals from 0.1 μm to 6 mm, *Phys. Earth Planet. Inter., 93*, 239-256, 1996.

Hunt, C. P., B. M. Moskowitz, and S. K. Banerjee, Magnetic properties of rocks and minerals, in *Rock Physics and Phase Relations: A Handbook of Physical Constants, AGU Ref. Shelf Ser.*, vol. 3, edited by T. J. Ahrens, pp. 189-204, AGU, Washington, D. C., 1995.

Jaep, W. F., Anhysteretic magnetization of an assembly of single-domain particles, *J. Appl. Phys., 40*, 1297-1298, 1969.

Jaep, W. F., Role of interactions in magnetic tapes, *J. Appl. Phys., 42*, 2790-2794, 1971.

King, J., S. K. Banerjee, J. Marvin, and Ö. Özdemir, A comparison of different magnetic methods for determining the relative grain size of magnetite in natural materials: Some results from lake sediments, *Earth Planet. Sci. Lett., 59*, 404-419, 1982.

King, J., S. K. Banerjee, and J. Marvin, A new rock-magnetic approach to selecting sediments for geomagnetic paleointensity studies: Application to paleointensity for the last 4000 years, *J. Geophys. Res., 88*, 5911-5921, 1983.

Levi, S., Some magnetic properties of magnetite as a function of grain size and their implications for paleomagnetism, Ph.D. thesis, Univ. of Washington, Seattle, 1974.

Levi, S., and R. T. Merrill, A comparison of ARM and TRM in magnetite, *Earth Planet. Sci. Lett., 32*, 171-184, 1976.

Levi, S., and R. T. Merrill, Properties of single-domain, pseudo-single-domain, and multidomain magnetite, *J. Geophys. Res., 83*, 309-323, 1978.

Maher, B. A., Magnetic properties of synthetic submicron magnetites, *Geophys. J., 94*, 83-96, 1988.

Moon, T. S., and R. T. Merrill, The magnetic moments of non-uniformly magnetized grains, *Phys. Earth Planet. Inter., 34*, 186-194, 1984.

Néel, L., Théorie du traînage magnétique des ferromagnétiques en grain fins avec applications aux terres cuites, *Ann. Géophys., 5*, 99-136, 1949.

Néel, L., Some theoretical aspects of rock magnetism, *Adv. Phys., 4*, 191-243, 1955.

Newell, A. J., D. J. Dunlop, and W. Williams, A two-dimensional model of magnetizations and fields in magnetite, *J. Geophys. Res., 98*, 9533-9549, 1993.

Özdemir, Ö., and S. K. Banerjee, A preliminary magnetic study of soil samples from west-central Minnesota, *Earth Planet. Sci. Lett., 59*, 393-403, 1982.

Özdemir, Ö., S. Xu, and D. J. Dunlop, Closure domains in magnetite, *J. Geophys. Res., 100*, 2193-2209, 1995.

Parry, L. G., Magnetic properties of dispersed magnetite powders, *Philos. Mag., 11*, 303-312, 1965.

Potter, D. K., and A. Stephenson, The detection of fine particles of magnetite using anhysteretic and rotational remanent magnetizations, *Geophys. J. R. Astron. Soc., 87*, 569-582, 1986.

Rahman, A. A., A. D. Duncan, and L. G. Parry, Magnetization of multidomain magnetite particles, *Riv. Ital. Geofis., 22*, 259-266, 1973.

Robins, B. W., Remanent magnetization in spinel iron oxides, Ph.D. thesis, Univ. of New South Wales, Sydney, Australia, 1972.

Roquet, J., Sur les rémanences des oxydes de fer et leur intérêt en géomagnétisme, *Ann. Géophys., 10*, 226-247 and 282-325, 1954.

Schmidbauer, E., and N. Schembera, Magnetic hysteresis properties and anhysteretic remanent magnetization of spherical Fe_3O_4 particles in the grain size range 60-160 nm, *Phys. Earth Planet. Inter., 46*, 77-83, 1987.

Schmidbauer, E., and R. J. Veitch, Anhysteretic remanent magnetization of small multidomain Fe_3O_4 particles in a non-magnetic matrix, *J. Geophys., 48*, 148-152, 1980.

Stacey, F. D., Thermoremanent magnetization (TRM) of multidomain grains in igneous rocks, *Philos. Mag., 3*, 1391-1401, 1958.

Stacey, F. D., The Koenigsberger ratio and the nature of thermoremanence in igneous rocks, *Earth Planet. Sci. Lett.*, 2, 67-68, 1967.

Stacey, F. D., and S. K. Banerjee, *The Physical Principles of Rock Magnetism*, 195 pp., Elsevier, New York, 1974.

Stephenson, A., and D. W. Collinson, Lunar magnetic field paleointensities determined by an anhysteretic remanent magnetization method, *Earth Planet. Sci. Lett., 23*, 220-228, 1974.

Sugiura, N., ARM, TRM and magnetic interactions: Concentration dependence, *Earth Planet. Sci. Lett., 42*, 451-455, 1979.

Thomson, L. C., R. J. Enkin, and W. Williams, Simulated annealing of three-dimensional micromagnetic structures and simulated thermoremanent magnetization, *J. Geophys. Res., 99*, 603-609, 1994.

Williams, W., and D. J. Dunlop, Three-dimensional micromagnetic modelling of ferromagnetic domain structure, *Nature, 337*, 634-637, 1989.

Williams, W., and D. J. Dunlop, Some effects of grain shape and varying external magnetic fields on the magnetic structure of small grains of magnetite, *Phys. Earth Planet. Inter., 65*, 1-14, 1990.

Williams, W., and D. J. Dunlop, Simulation of magnetic hysteresis in pseudo-single-domain grains of magnetite, *J. Geophys. Res., 100*, 3859-3871, 1995.

Worm, H-U., *Herstellung und magnetische Eigenschaften kleiner Titanomagnetit-Ausscheidungen in Silikaten*, Ph.D. thesis, Univ. Bayreuth, Bayreuth, Germany, 1986.

Xu, S., and R. T. Merrill, The demagnetizing factors in multidomain grains, *J. Geophys. Res., 92*, 10,657-10,665, 1987.

K. S. Argyle, Arlat Inc., 150 East Drive, Bramalea, Ontario, Canada L6T 1C1.

D. J. Dunlop, Department of Physics, University of Toronto at Mississauga, 3359 Mississauga Road North, Mississauga, Ontario, Canada L5L 1C6. (e-mail: dunlop@physics.utoronto.ca)

(Received October 18, 1996; revised March 20, 1997;
accepted March 28, 1997.)